Corrosion Science 251 (2025) 112896

Contents lists available at ScienceDirect

Corrosion Science

journal homepage: www.elsevier.com/locate/corsci

Influence of aluminizing and pre-oxidation on corrosion behavior of 316Ti in liquid Pb at 600–700 °C

Anisa Purwitasari [a], Renate Fetzer [a,*], Annette Heinzel [a], Ceyhun Oskay [a,b], Alfons Weisenburger [a], Georg Müller [a]

[a] Institute for Pulsed Power and Microwave Technology (IHM), Karlsruhe Institute of Technology (KIT), Hermann-von-Helmholtz-Platz 1, Eggenstein-Leopoldshafen 76344, Germany
[b] DECHEMA-Forschungsinstitut, Theodor-Heuss-Allee 25, Frankfurt am Main 60486, Germany

ARTICLE INFO

Keywords:
Corrosion
Austenitic steel
Liquid lead
Surface aluminizing
Pack cementation
Pre-oxidation

ABSTRACT

This study explores the possibility to extend the service temperature of austenitic steel 316Ti in liquid lead to 700 °C. To improve the material compatibility, 316Ti is subjected to three different pre-treatments prior to Pb exposure: pre-oxidation in hot air, aluminizing by pack cementation, and the combination of both. In exposure tests with duration up to 5000 hours, the combined pre-treatment comprising aluminizing by pack cementation and subsequent pre-oxidation is found to provide the most effective corrosion protection to austenitic steel 316Ti in contact with liquid Pb containing 2×10^{-7} wt% dissolved oxygen at both 600 and 700 °C.

1. Introduction

Liquid metals are gaining attention as potential cooling fluids for advanced fast reactor systems and as heat transfer fluids in thermal energy storage (TES) for waste heat recovery and process heat from renewable energy sources. Their excellent thermal properties and high boiling points enable high heat transfer rates and operation over a wide temperature range. Among liquid metals, liquid lead (Pb) stands out due to its high availability and low cost, making it a cost-effective option. Furthermore, Pb has no intense reactivity with water or air, which poses a significant advantage over, e.g., Na. Additionally, its low vapor pressure ensures stability at high temperatures, and its low neutron capture cross-section adds further benefits in nuclear applications [1–5]. However, the use of liquid Pb and Pb alloys presents significant challenges due to their highly corrosive nature, particularly at elevated temperatures. Exposure of austenitic steels in liquid metals at high temperatures under various oxygen concentrations has been reported to cause changes in surface morphology and microstructural changes or ferritization due to selective dissolution of austenite stabilizing alloying constituents such as Ni [6]. Therefore, careful material selection for critical components such as pumps and valves is crucial, as these parts are essential for maintaining operational reliability and ensuring safe operating conditions.

One of the prevalent types of austenitic steel used in pump and valve manufacturing is 316 grade, as it is known for its excellent strength and corrosion resistance at high temperatures. A modified version, 316Ti, is stabilized with titanium, offers enhanced strength, and prevents sensitization or carbide precipitation—a common issue in standard 316 stainless steel that can lead to intergranular corrosion. While extensive data on the corrosion behavior of 316 steel in liquid lead-bismuth eutectic (LBE) at temperatures up to 800 °C is available, data on the corrosion behavior of 316Ti in liquid Pb is limited. Most studies reported that 316 steel is vulnerable to corrosion phenomena such as the dissolution of alloying constituents and liquid metal attacks at temperatures higher than 600 °C [7–11].

A common strategy to inhibit corrosion in liquid Pb or LBE is to develop a protective barrier on the steel surface, which prevents direct contact between the steel and liquid metal. A straightforward treatment for creating this barrier is pre-oxidation. Maia et al. revealed that bare 316 L steel underwent dissolution corrosion in liquid LBE at 400 °C with an oxygen concentration of 10^{-9} to 10^{-10} wt%. Pre-oxidation prior to exposure at different temperatures led to the formation of an outer Fe-rich oxide layer and an inner Fe-Cr spinel layer, which shifted the corrosion mechanism to localized pitting [12]. Another investigation involved different alumina forming austenitic (AFA) steels and ferritic FeCrAlMo alloy with different liquid metals. Pre-oxidation improved the compatibility of the AFA steels with liquid metal Pb after 1000 h exposure at a temperature of 700 °C. A significant reduction in mass loss and

* Corresponding author.
E-mail address: renate.fetzer@kit.edu (R. Fetzer).

https://doi.org/10.1016/j.corsci.2025.112896
Received 2 January 2025; Received in revised form 26 March 2025; Accepted 27 March 2025
Available online 29 March 2025

no evidence of dissolution were observed in pre-oxidized samples [13]. Pre-oxidation seems to be beneficial especially for the short-term behavior. However, for long-term performance, it is crucial that an oxide layer can self-heal during exposure in case of mechanical damage to the scale such as crack formation or spallation. Essential for the in-situ oxide formation is the introduction of oxygen into the liquid metal. The oxygen content has to be high enough to allow a fast oxide formation on the steel surfaces at all operating temperatures, but low enough to prevent Pb-oxide formation. Using strong oxide formers like Al and Si enlarges the operation windows of the oxygen content, since Al-oxide and Si-containing spinel have a lower oxidation potential than magnetite or Fe-Cr spinel, i.e., a lower oxygen content suffices for their formation. Especially Al is known to be oxidized selectively and to form dense and slowly-growing oxide layers. Therefore, alumina-forming alloys are in the focus for high temperature applications in heavy liquid metals [14–17].

Despite the research on alumina-forming alloys, 316-type steels remain at present the prevalent choice for pumps and valves. Since 316Ti is, like many austenitic steels, not an alumina-forming material, applying an Al-rich coating is necessary. Such coatings can be classified in two groups, (i) overlay coatings applied by a deposition method like plasma spraying without further treatment, (ii) surface modification methods. To overcome the issues related with a non-perfect adhesion of deposited coatings, surface modification methods such as diffusion coatings are preferred. For a diffusion coating, Al is deposited to the surface and diffused into the steel surface at a higher temperature, which enables an optimal connection to the base material by forming intermetallic phases. One method to apply Al for subsequent diffusion is hot dipping. This type of Al diffusion coating was mainly developed for nuclear fusion reactors to reduce the corrosion and the tritium permeation in the first wall [18,19]. However, the applied Al layer thickness is difficult to control. The high amount of Al led to an excessively high Al content on the surface, which, due to the high solubility in liquid Bi, led to dissolution attack instead of the formation of protective oxide layers when exposed to flowing LBE, even at 420 °C [20,21]. This showed that the Al concentration on the steel surface is crucial for formation of a protective oxide layer. If the activity of Al is not high enough, the formation of fast-growing and non-protective scales due to the oxidation of steel alloying elements cannot be suppressed. A promising result showed the Al foil wrapping method [21,22], but this method cannot be used with more complex structures and fails if the foil is not sticking well on the steel surface. A possible solution is the industrially well-established pack cementation method. It is an in-situ chemical vapor deposition method with simultaneous diffusion and formation of Al-rich intermetallics. Diffusion aluminizing is a generally used method to improve the oxidation/corrosion behavior of steels in oxidizing atmospheres [23–26] or in molten salts [27–29] at high temperatures. On the other hand, to the authors' knowledge, there aren't many studies investigating the corrosion resistance of such coatings in liquid Pb at high temperatures. Deloffre et al. [30] tested aluminized martensitic and austenitic (316 L) steels by pack cementation at temperatures between 350 °C and 600 °C in stagnant and flowing LBE with different oxygen contents. In stagnant condition, the aluminized 316 L showed no change of the coating up to 500 °C and 10.000 h in LBE with an oxygen concentration of 10^{-9} to 10^{-8} wt%. The oxygen content becomes more important at higher temperatures. At 600 °C, corrosion attack occurred below 10^{-8} wt% oxygen, while above 10^{-8} wt% no changes of the coating were observed in stagnant conditions and flowing conditions (1.9 m/s) caused changes only in areas with turbulent flow. Pack-cementation was also applied to Ni-based Inconel 625, which is prone to Ni dissolution and LBE penetration, to create a NiAl-rich coating. The aluminized Inconel 625 exhibited an Al-rich oxide layer and good compatibility with LBE at 600 °C after 200 h. However, at 850 °C for 72 h, it underwent LBE penetration and dissolution corrosion [31].

These results indicate that at elevated temperatures the kinetics of Pb/LBE penetration and dissolution corrosion outweighed the alumina formation. Hence, it may be required to perform the alumina formation before the exposure in liquid metal, i.e., to introduce a pre-oxidation step.

With increasing interest in using liquid Pb for high-temperature applications above 600 °C, further research is needed, as first studies indicate corrosion of 316Ti under prolonged exposure at these temperatures [11]. Since pre-treatments promise an improvement of the corrosion resistance, this study focuses on examining the corrosion behavior of 316Ti with three selected pre-treatments at two temperatures, 600 °C and 700 °C, and over exposure times of up to 5000 h. The oxygen concentration for all experiments is set at 2×10^{-7} wt%, which allows formation of Fe spinel, Cr-oxides, and Al-oxides.

2. Materials and methods

2.1. Materials and pre-treatments

In this study, commercially available austenitic steel AISI 316Ti (1.4571) is pre-treated and subsequently tested in static liquid Pb. Its measured chemical composition as provided by the supplier is shown in Table 1.

The 316Ti specimens were cut into rectangular coupons with a dimension of 29 mm× 10 mm x 2 mm. A hole was drilled into one side of each specimen. Before starting the pre-treatments, the specimens were ground using 1200# SiC grinding paper and then cleaned in ethanol.

Three different pre-treatments were applied to the 316Ti substrate to form a corrosion inhibitor layer prior to exposure in liquid Pb. The first treatment involved pre-oxidation at high temperature to form a Cr-rich oxide layer on the surface. The second treatment was aluminizing via pack cementation to develop an aluminide coating on the 316Ti substrate. The third treatment combined aluminizing by pack cementation with subsequent pre-oxidation. The original untreated 316Ti was also included in the exposure plan.

Diffusion aluminizing process was undertaken by in-pack cementation. Samples were initially glass-bead blasted and degreased in an ultrasonic acetone bath. Thereafter, they were embedded in alumina retorts in a pack powder mixture consisting of the diffusion element Al, the halide activator NH_4Cl, and the inert filler Al_2O_3 with the composition ratio of 1.5 wt%, 1 wt%, and 96 wt%, respectively. Thereafter, the retorts were placed in a furnace equipped with a quartz tube, which was evacuated and filled with Ar twice and then heated up to 150 °C under Ar/H_2 flow (Ar + 5 vol% H_2, 4 L/h) to reduce the oxygen content. Subsequently, the coating manufacturing process was conducted at 1000 °C for 1.5 h under the above-mentioned gas flow. The samples were cooled down to room temperature, removed from the retorts, and cleaned in ultrasonic acetone bath. Further details on the coating manufacturing process can be found in [32–35].

Pre-oxidation treatment was conducted in still laboratory air in a muffle furnace at 1000 °C for 4 h to initiate the formation of a Cr-rich oxide scale on the uncoated 316Ti and an Al-rich oxide scale on the aluminized samples prior to the exposure in liquid Pb. The temperature of 1000 °C was chosen to enable the formation of stable α-alumina on the aluminized samples. The samples were cooled down in the furnace, i.e., the cooling rate was rather low.

Fig. 1 summarizes X-ray diffraction (XRD) patterns of untreated 316Ti, pre-oxidized 316Ti, aluminized 316Ti, and aluminized and subsequently pre-oxidized 316Ti prior to exposure to liquid Pb. The diffraction pattern of untreated 316Ti shows an austenitic microstructure with a small ferrite content, which stems from δ-ferrite stringers present in the bulk material [11]. The XRD results of pre-treated 316Ti confirm the successful application of the respective pre-treatments, i.e., the formation of Cr_2O_3 during pre-oxidation of pristine 316Ti, the formation of an FeAl intermetallic phase during aluminizing, and the formation of α-Al_2O_3 (corundum) during subsequent pre-oxidation.

Fig. 2a shows a representative cross-sectional SEM-BSE

Table 1
Chemical composition of austenitic steel 316Ti in wt%.

Material	C	Si	Mn	S	Cr	Ni	Mo	N	Ti	Fe
316Ti	0.030	0.36	1.11	0.004	16.70	10.50	2.02	0.013	0.381	bal.

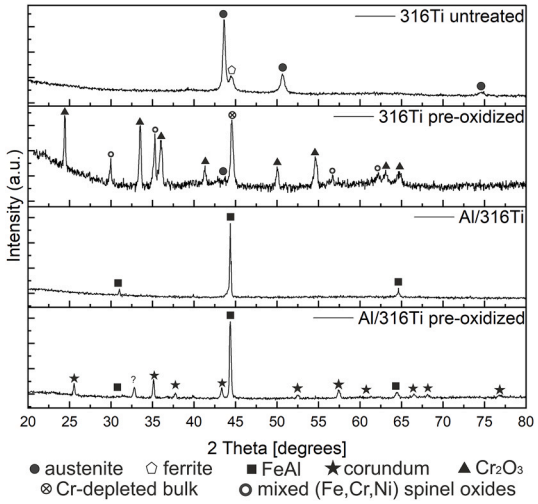

Fig. 1. XRD results of 316Ti in untreated, pre-oxidized, aluminized, and pre-oxidized aluminized condition.

(backscattered electrons) image of 316Ti after pre-oxidation, revealing non-uniform oxide formation at the sample surface and internal oxidation within the bulk. An overview image with lower magnification can be found in the Supplementary Material, Fig. S2a. The left part of Fig. 2a exhibits a thin oxide layer formation with a thickness of approximately 3 μm. According to the EDS line scan 1 across the thin oxide layer (see Fig. 2c), the oxide contains primarily Cr with no presence of other elements, suggesting the formation of a Cr-rich oxide, which is confirmed as Cr_2O_3 by the XRD results presented in Fig. 1. On the other hand, the right part of Fig. 2a represents a local breakaway and shows a porous oxidized zone with a greater depth, reaching up to 30 μm. In other locations, the thick oxide reaches up to 50 μm (Fig. S2a). EDS line scan 2 across the thick and porous inward-growing oxide (see Fig. 2d) shows that the oxide contains Fe, Cr and Ni, suggesting the formation of a Fe-Cr-Ni spinel as confirmed by the XRD results (Fig. 1). Moreover, a Si peak is observed beneath the Cr-rich oxide in both line scans, which indicates the formation of a Si-rich oxide at the interface to the bulk. The EDS line scans and EDS elemental mapping (see Fig. 2b-d) further reveal a higher Cr concentration within the innermost oxide layer right at the bulk interface, while a clear Cr depletion is observed in the bulk below due to the consumption of Cr for oxide formation. The Cr depletion combined with the low cooling rate after pre-oxidation leads to ferritization of the surface-near bulk, see EBSD phase mapping in Fig. 2e and f and respective diffraction peak denoted Cr-depleted bulk in Fig. 1.

Fig. 3 presents the cross-sectional analysis of 316Ti after aluminizing via pack cementation (see Fig. S3a for an image with lower magnification). A uniform coating layer with a typical high activity coating microstructure [36,37] is formed on the 316Ti substrate, comprising an outer layer (diffusion zone, DZ) with a thickness of ~40 μm and an interdiffusion zone (IDZ) with a thickness of ~55 μm. Both horizontal and vertical cracks are present in the outer layer, which are formed during the cooling process of the pack aluminizing. Their presence can be attributed to the build-up of thermally induced stresses during cooling down due to the mismatch of thermal expansion coefficients between the Al-rich coating and the substrate [38,39]. The peaks revealed by XRD analysis of the aluminized 316Ti (Fig. 1) could be identified as B2-FeAl, a non-stoichiometric intermetallic phase with wide homogeneity range (~25–52 at% Al at 1000 °C). According to the line measurement in Fig. 3b, the outer layer contains also Cr and Ni, which indicates a solid solution (Fe,Cr,Ni)Al with an ordered B2 structure. The EDS line scan in Fig. 3b also shows that the Al concentration in the outer and IDZ layers generally decreases with depth. The Ni concentration increases with depth in the outer layer, reaching around 28 at % in the innermost region of the DZ, right at the interface with the IDZ. Here, a continuous Ni-rich intermediate layer is formed, see also the EDS

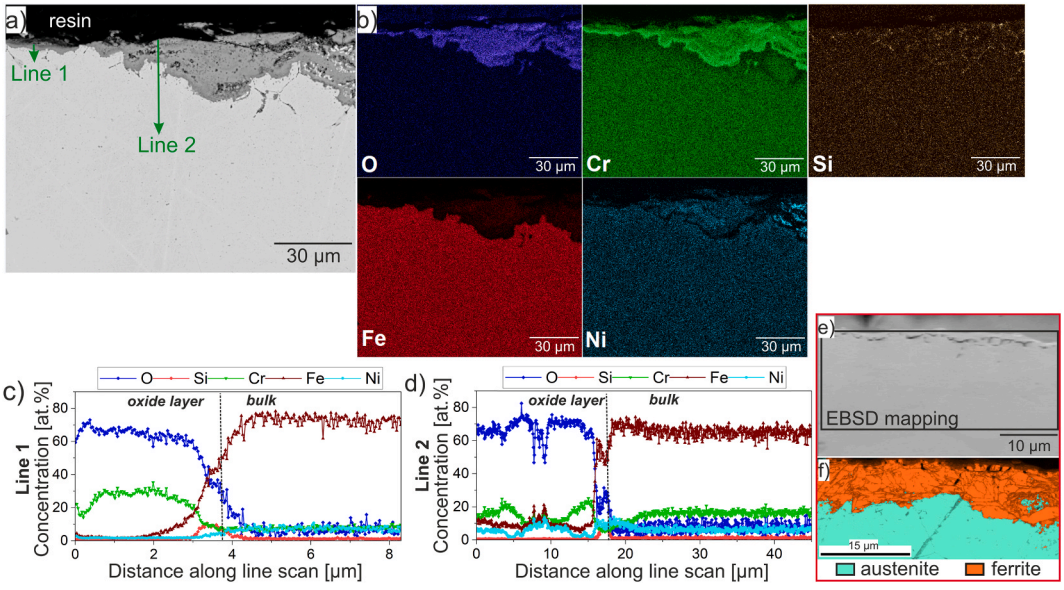

Fig. 2. As pre-oxidized 316Ti. a) and b) represent BSE image and its EDS elemental distribution mappings, c) EDS line scan result across the thin oxide layer (see line 1 in a), d) EDS line scan result across the thicker and porous oxidized zone (see line 2 in a), e) EBSD mapping location at position with thin oxide scale, and f) EBSD phase mapping result.

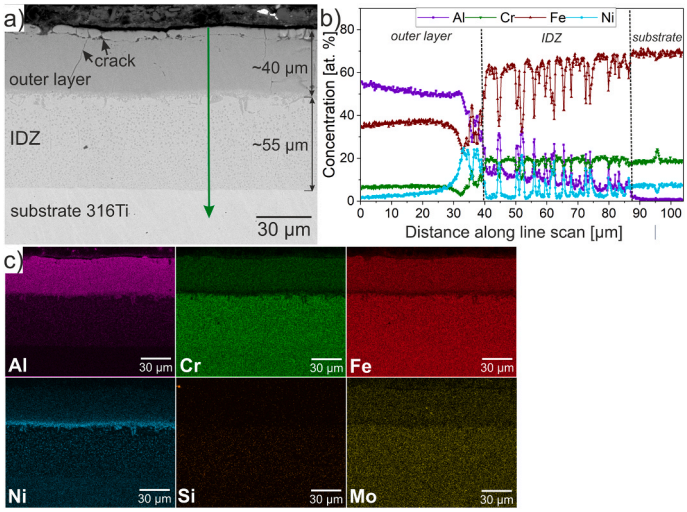

Fig. 3. As aluminized 316Ti via pack cementation. a) BSE image, b) EDS line scan result across the outer layer, IDZ and substrate (see the green arrow a) and c) EDS elemental distribution mapping.

elemental mapping in Fig. 3c. This is a quite common observation for diffusion aluminide coatings deposited on austenitic steels. It is explained by the outward diffusion of Ni from the substrate, the inward diffusion of Al towards the substrate, and the high affinity between Ni and Al [40]. The IDZ layer shows finely dispersed B2-NiAl precipitates that are embedded in an Fe- and Cr-rich ferritic matrix. The outward diffusion of Ni and the formation of the B2-precipitates in the IDZ lead to a Ni depletion in the matrix of the IDZ zone, which causes destabilization of the austenitic microstructure and its transformation to ferrite [41].

Fig. 4a, b, and d show BSE images of the aluminized 316Ti specimen after pre-oxidation (a low-magnification image is presented in Fig. S4a). An alumina layer with a varying thickness of 3–9 µm is formed on the aluminide coating, see also corresponding elemental mapping result in Fig. 4f. Formation of the targeted corundum or α-Al_2O_3 after 4 h pre-oxidation at 1000 °C is confirmed by XRD analysis, see Fig. 1. The upper part of the alumina layer shows horizontal cracks (see Fig. 4b), likely resulting from the preparation steps. Some cracks originating from the pack cementation process are found to be filled with Al-rich oxide. Beneath the alumina layer, voids are formed due to the Kirkendall effect caused by the different diffusion rates of the elements.

Two distinct outer layer microstructures are observed throughout the sample coating. Fig. 4b depicts a region where the outer layer is homogeneous, see also the corresponding line scan results in Fig. 4c. The analysis reveals a significant reduction in Al concentration compared with the outer layer prior to pre-oxidation (Fig. 3b), which is caused by Al consumption in the alumina formation and Al diffusion towards the substrate. The decrease of the Al content to approximately 26 at% is accompanied by an Fe increase to ~57 at% and slightly higher Ni and Cr concentrations. Despite the lower Al concentration, the outer layer still shows the B2-FeAl microstructure, see XRD results in Fig. 1. At another location of the sample, depicted in Fig. 4d with the corresponding EDS line scan in Fig. 4e, the outer layer shows decomposition into a matrix

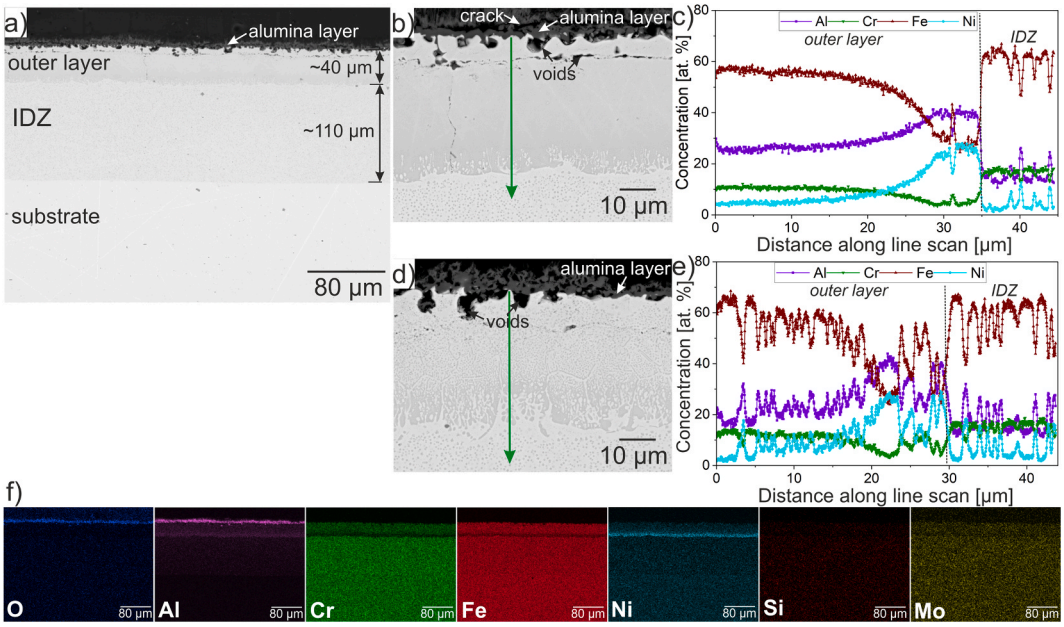

Fig. 4. Aluminized 316Ti after pre-oxidation. a) BSE image of the coating and substrate, b) BSE image of a homogeneous outer layer, c) EDS line scan result along green arrow in b), d) BSE image of an outer layer with markedly microstructural evolution, e) EDS line scan result along green arrow in d), f) EDS elemental distribution mapping of a).

and dispersed NiAl precipitates. The strong affinity between Ni diffusing from the substrate and Al leads to the formation of NiAl, which results in a further reduction of Al in the matrix and destabilization of the B2-FeAl structure. The Al content of the matrix is measured to be 18–20 at%, which suggests formation of a ferritic α-Fe structure. The observed microstructural variations along the sample may be attributed to differences in local diffusion activities or Al uptake during the pack cementation process, which is known to depend critically on local sample properties, surface finish, and process parameters. The IDZ has increased in thickness from 55 μm to 110 μm after pre-oxidation. It consists of a ferritic matrix and finely dispersed spherical NiAl precipitates.

2.2. Corrosion tests

The stagnant corrosion tests were carried out in the COSTA facility developed at Karlsruhe Institute of Technology (KIT) [42]. The facility consists of a furnace with a quartz glass tube and a gas control system. Liquid Pb was filled in alumina crucibles and inserted in the tube. The amount of oxygen dissolved in the liquid Pb was controlled via the gas phase by a continuous flow of Ar and Ar/H_2 with a specific H_2/H_2O ratio. After several days of conditioning, an equilibrium between the oxygen activities in the gas atmosphere and in the liquid Pb was achieved and the specimens were inserted. To prevent oxygen break-in during specimen loading and unloading, a pre-conditioned glove box was employed. The specimens were mounted with a Mo-wire to alumina holders and then immersed in the alumina crucibles filled with the conditioned liquid Pb. Each crucible contained one specimen. During the entire exposure tests, the oxygen partial pressure of the gas leaving the quartz glass tube was monitored using a high-precision oxygen analyzer (SGMT1.3 from ZIROX, Germany). From these data, the oxygen concentration in liquid Pb was calculated using the oxygen saturation data reported in Ref. [43].

The corrosion tests were performed at 600 and 700 °C. The targeted oxygen concentration in the liquid Pb for both temperatures was 2×10^{-7} wt%. Table 2 outlines the exposure plans and durations for the different pre-treated materials. The monitored oxygen content over the exposure time is shown in Fig. 5.

2.3. Post-exposure examination

After the corrosion tests, the specimens were cut longitudinally into two parts. The first part was used for cross-sectional analysis, while the second part was kept for X-ray diffraction (XRD) analysis. The first part was cold-mounted in resin without a preliminary cleaning step. The embedded samples were ground with up to 2400# SiC paper and polished with a diamond suspension down to 1 μm. For a better conductivity, the samples were then sputtered with a thin layer of gold. Scanning electron microscopy (SEM, Zeiss LEO 1530 VP) equipped with EDS (IDFix, SAMx) and electron backscatter diffraction (EBSD, EDAX) were used to characterize the materials and coatings prior to and after Pb exposure. Hereby, the corrosion behavior was analyzed at different locations on the sample to ensure consistent exposure conditions, in particular a homogeneous oxygen concentration in the liquid Pb. EBSD analysis was performed to investigate any potential evolution of the microstructure after exposure. Prior to EBSD analysis, the samples were further polished using a vibration polisher (Buehler Vibromet 2) with colloidal SiO_2 polishing fluid. The EBSD mapping results were analyzed using the OIM Analysis software from EDAX. The second half of each exposed sample was analyzed using X-ray diffraction (XRD, Seifert 3003 PTS) with Cu $K_{\alpha 1}$ radiation to characterize the coating layer and the oxides formed. Before conducting XRD analysis, the exposed samples were cleaned from adherent lead by immersing them in a 1:1:1 mixture of acetic acid, hydrogen peroxide, and ethanol, followed by rinsing with distilled water and ethanol.

3. Results

3.1. Untreated 316Ti

Results of exposure tests of 316Ti without any pre-treatment in liquid Pb at 600 and 700 °C are published in detail in a recent study, to which the readers are referred for further details [11]. Due to their relevance for the present study, where the influence of different pre-treatments is assessed, the main results of untreated 316Ti are summarized in the following. Cross-sectional BSE (backscattered electron) images of the untreated 316Ti specimen after 5000 h of exposure in liquid Pb at 600°C are shown in Fig. S1a (low magnification) and in Fig. 6a. The untreated 316Ti specimen exhibits liquid Pb penetration to a depth of up to 80 μm, along with evidence of Ni and Cr depletion in the subsurface, indicating dissolution corrosion (see mappings in Fig. 6c). The dissolution of Ni as an austenite stabilizer leads to subsurface ferritization, as confirmed by the EBSD mapping result shown in Fig. 6b. The XRD results in Fig. 7 indicate that the austenite peak in the sample before exposure has transformed into ferrite peaks after exposure at 600 °C. Dissolution corrosion and liquid Pb penetration were already apparent after 1000 h and 2000 h of exposure, see Ref. [11].

Fig. 8a shows a representative cross-sectional BSE image of the untreated 316Ti after 2000 h exposure in liquid Pb at a higher temperature of 700 °C. A thin, inward growing oxide layer is observed in some regions. The XRD results shown in Fig. 7 reveal the oxides formed after 2000 h of exposure at 700 °C as Fe-Cr spinel and Cr_2O_3. However, this layer appears discontinuous and shows signs of local detachment (see red arrow in Fig. 8a). As shown in Ref. [11], EDS elemental distribution mapping reveals significant Ni depletion and minor Cr depletion in the area beneath the detachment region, leading to subsurface ferritization as confirmed by XRD results in Fig. 7. After 5000 h of exposure (see Fig. 8b and the low-magnification images in Fig. S1b), the oxide layer is no longer visible, suggesting that the layer has completely delaminated and the material is unable to re-form the scale. Instead, the dissolution of alloying elements such as Ni (see EDS elemental mapping in Fig. 8d) results in subsurface ferritization as validated by the EBSD phase mapping result presented in Fig. 8c and the XRD results presented in Fig. 7. Despite the severe dissolution corrosion observed at the subsurface, no liquid Pb penetration is apparent. Besides TiN precipitates, Cr-rich sulfide precipitates are found within the ferrite zone, while in the bulk below patches of a Cr-Mo-rich σ-phase are formed, see also [11].

3.2. Pre-oxidized 316Ti

Fig. 9a shows a typical cross-sectional BSE image of the pre-oxidized 316Ti specimen after 5000 h of exposure in liquid Pb at 600 °C, while an

Table 2
Different pre-treatments and exposure plan for 316Ti.

Material	600 °C			700 °C		
	1000 h	2000 h	5000 h	1000 h	2000 h	5000 h
Untreated 316Ti	✓	✓	✓	✓	✓	✓
316Ti pre-oxidized			✓			✓
Aluminized 316Ti	✓	✓		✓	✓	
Aluminized 316Ti pre-oxidized			✓			✓

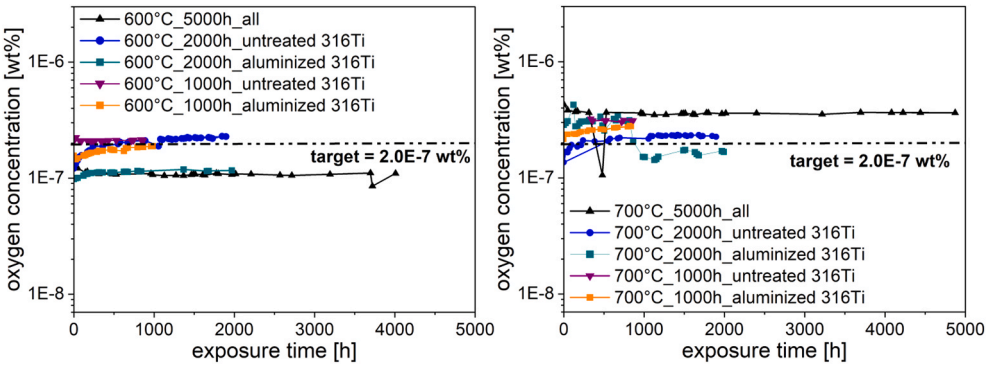

Fig. 5. Monitored oxygen concentration during the exposure tests. Left: tests at 600 °C, right: test at 700 °C. The data for the 5000 h exposures apply to all three samples, i.e., untreated 316Ti, pre-oxidized 316Ti, and aluminized 316Ti pre-oxidized.

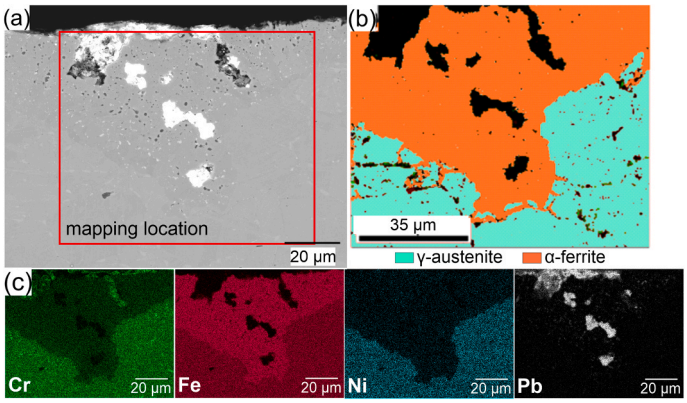

Fig. 6. Untreated 316Ti after 5000 h of exposure in liquid Pb at 600 °C. a) BSE image, b) EBSD phase mapping result and c) EDS elemental distribution mapping of a).

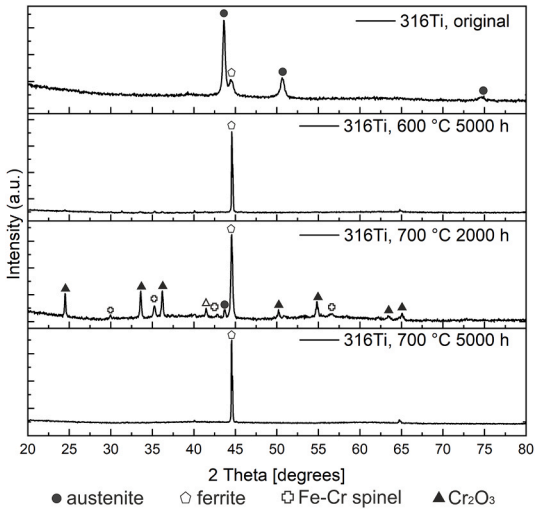

Fig. 7. XRD results of untreated 316Ti before and after exposures in liquid Pb at 600 °C and 700 °C.

image with lower magnification is presented in Fig. S2b. Liquid Pb is found to be present within the porous structure of Fe-Cr-Ni spinel, but has not yet penetrated the bulk. The oxide layer on the sample surface appears unchanged compared to its as-pre-oxidized state shown in Fig. 2a, indicating no deterioration of the oxide layer. According to the line scan in Fig. 9b, no depletion of Ni is detected beneath the oxide layer, indicating that the pre-oxidation could effectively prevent the dissolution of Ni up to 5000 h at 600 °C.

Fig. 10a shows a representative cross-sectional BSE image of the pre-oxidized 316Ti specimen after 5000 h of exposure in liquid Pb at 700 °C (see Fig. S2c for an image with lower magnification). The sample shows two regions. On the left, the oxide formed during pre-oxidation is still present. Liquid Pb infiltrates the porous structure of the oxide layer, but no Ni depletion is observed in the bulk below. In the right part of Fig. 10a (see red arrow), liquid Pb adheres directly to the bulk, suggesting that the oxide layer has locally delaminated during exposure. An inward-growing oxide is visible throughout the entire sample to a depth of up to 130 µm, which is greater than the oxide depth observed in the initial, pre-oxidized state (50 µm, see Fig. S2a). The EDS elemental mapping in Fig. 10b indicates that Cr is selectively oxidized both in the area covered by the pre-formed oxide and in the area where the pre-formed oxide is detached, with Cr depletion observed in the space between the Cr-rich oxide. Despite the local detachment of the pre-formed oxide layer, no liquid Pb is found in the bulk beneath the detached region. This indicates that the inward-growing oxide is able to prevent the penetration of liquid Pb. However, depletion of Ni due to dissolution is observed in this region, which leads – in combination with the Cr depletion due to oxide formation – to ferritization, as confirmed by the EBSD phase mapping result in Fig. 10c.

3.3. *Aluminized 316Ti*

Fig. 11 presents the cross-sectional analysis of the aluminized 316Ti exposed to liquid Pb at 600 °C for 2000 h (similar behavior is observed after 1000 h, see Fig. S3b and c). No corrosion attack can be detected either in the coating layer or in the substrate. A ~400 nm thin oxide layer rich in Al is found on the coating layer after the exposure, as shown

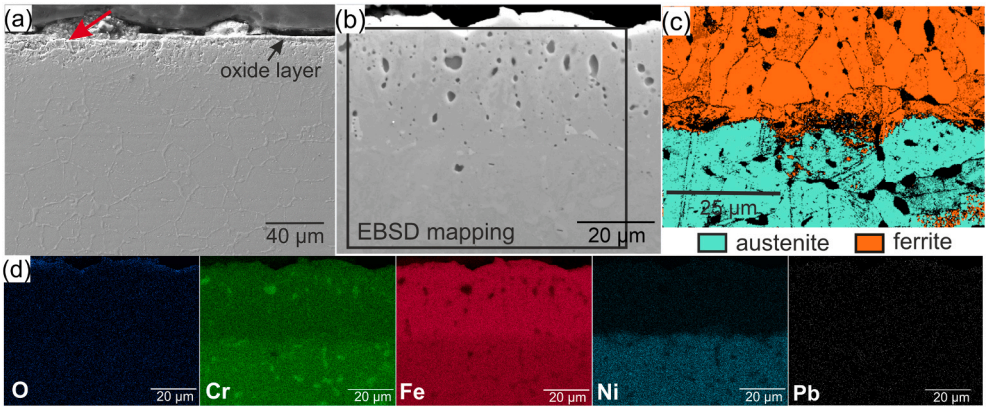

Fig. 8. Untreated 316Ti after exposure in liquid Pb at 700 °C. a) BSE image after 2000 h exposure b) SE image after 5000 h exposure, c) EBSD phase mapping result and d) EDS elemental distribution mappings of b).

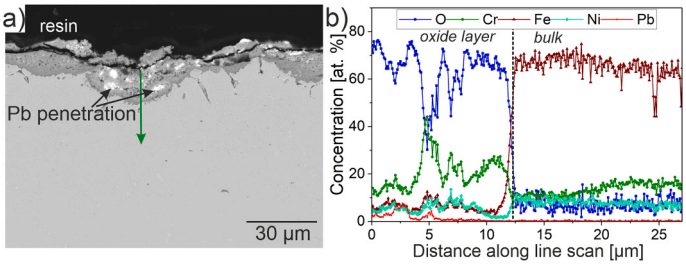

Fig. 9. Pre-oxidized 316Ti after 5000 h exposure in Pb at 600 °C. a) BSE image, b) EDS line scan results along the green arrow (see a).

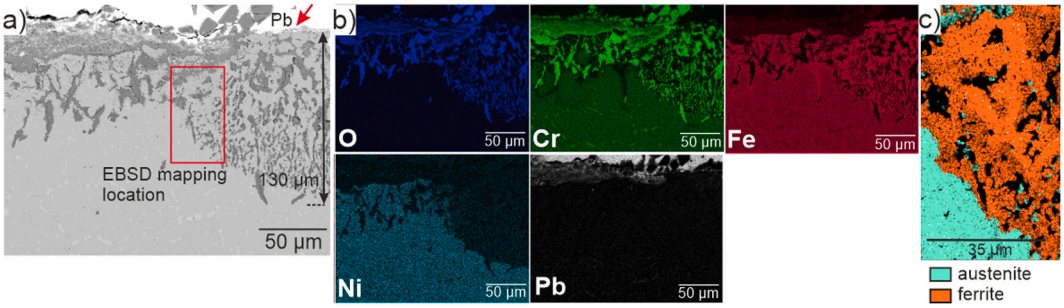

Fig. 10. Pre-oxidized 316Ti after 5000 h exposure in liquid Pb at 700 °C. a) and b) BSE image and its EDS elemental distribution mappings, and c) EBSD phase mapping.

in Fig 11a1. The EDS line scan in Fig. 11b reveals a slight decrease in aluminum content to 48 at% in the outer layer compared with the outer layer prior to Pb exposure (Fig. 3), along with a minor relative increase in Fe and Cr concentrations. The decrease in Al concentration of the outer layer is attributed to the formation and growth the oxide scale and, to a higher extent, to diffusion towards the bulk, leading to a significant increase of aluminum content in the interdiffusion zone. Dissolution of Al into the liquid Pb is inhibited by the thin oxide layer grown on the surface of the coating. Compared to the as-aluminized condition (see Fig. 3), despite the slight Al-depletion, the microstructure of the DZ remains almost unchanged. Unlike the DZ, the microstructure of the IDZ shows significant differences compared to the as-aluminized condition. Within the IDZ, Mo-Si-rich carbides (χ-phase) are formed along the grain boundaries of the ferritic matrix, as can be seen in Fig. 11a2 and in the elemental mapping in Fig. 11c. Coarse Cr-Mo-rich phases (σ-phase) are present along the interface between IDZ and substrate, where a transition zone (TZ) due to Al inward diffusion into the substrate is observed (see Fig. 11a2). The observed precipitation of both the χ-phase along the grain boundaries and the σ-phase at the transition to the bulk corresponds to a typical microstructural evolution of diffusion aluminide coatings for prolonged exposure at elevated temperature [44], irrespective of the corrosion processes at the surface.

Fig. 12a presents the aluminized 316Ti specimen exposed in liquid Pb at a higher temperature of 700 °C for 2000 h, along with its EDS elemental mapping in Fig. 12b. An image with lower magnification is shown in Fig. S3e. After 1000 h (Fig. S3d) and 2000 h of exposure, the aluminized sample suffers from severe liquid Pb penetration, reaching a depth of 130 µm after 1000 h and up to 180 µm after 2000 h exposure. This corrosion depth exceeds the total thickness of both the coating and the original IDZ, which was approximately 90 µm. The elemental mappings in Fig. 12b also reveal depletion of Ni and Al in the area surrounding the penetrated lead, hinting at a high level of dissolution of these elements into the liquid Pb. Additionally, the formation of a rather thick transition zone at the interface between IDZ and steel due to Al inward diffusion with a depth > 100 µm is observed, accompanied with the formation of NiAl and Cr-Mo-rich precipitates.

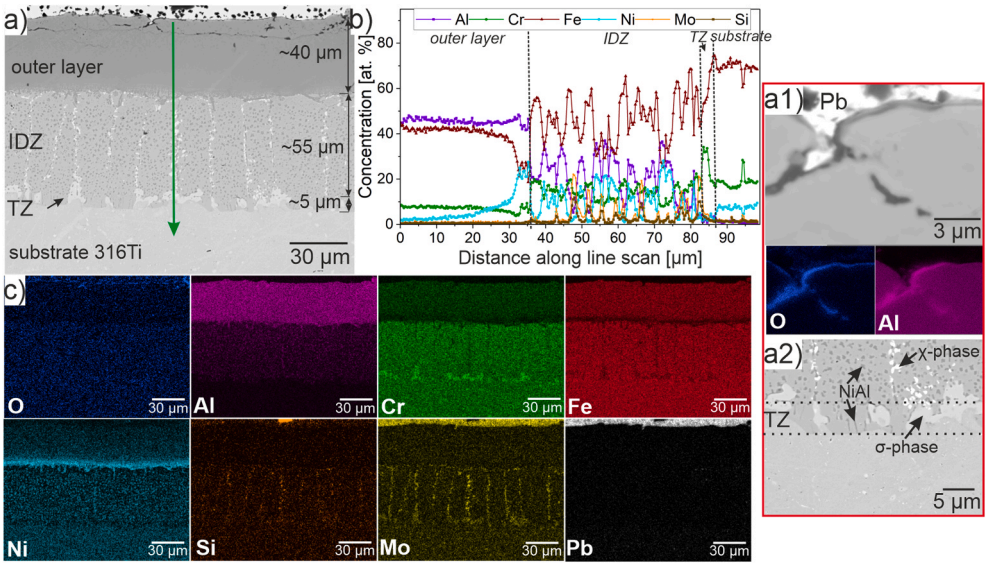

Fig. 11. Aluminized 316Ti after 2000 h of exposure in liquid Pb at 600 °C. a) BSE image, b) EDS line scan result across the outer layer, IDZ and the substrate (see green arrow in a), c) EDS elemental distribution mapping of a. Detail a1) enlarged section of oxide layer, detail a2) microstructure image with transition region.

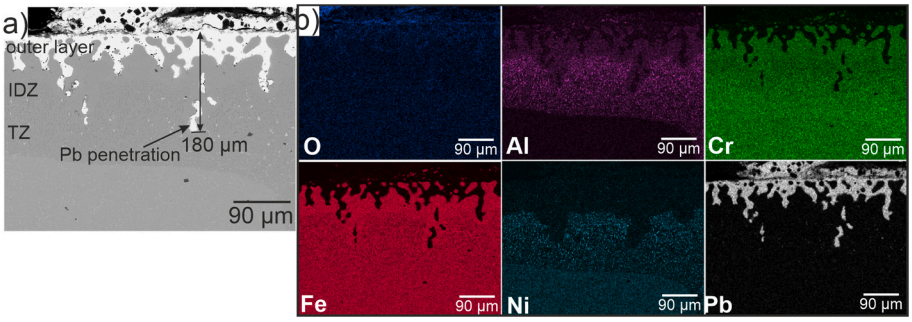

Fig. 12. Aluminized 316Ti after 2000 h exposure in liquid Pb at 700 °C. a) and b) BSE image its EDS elemental distribution mapping.

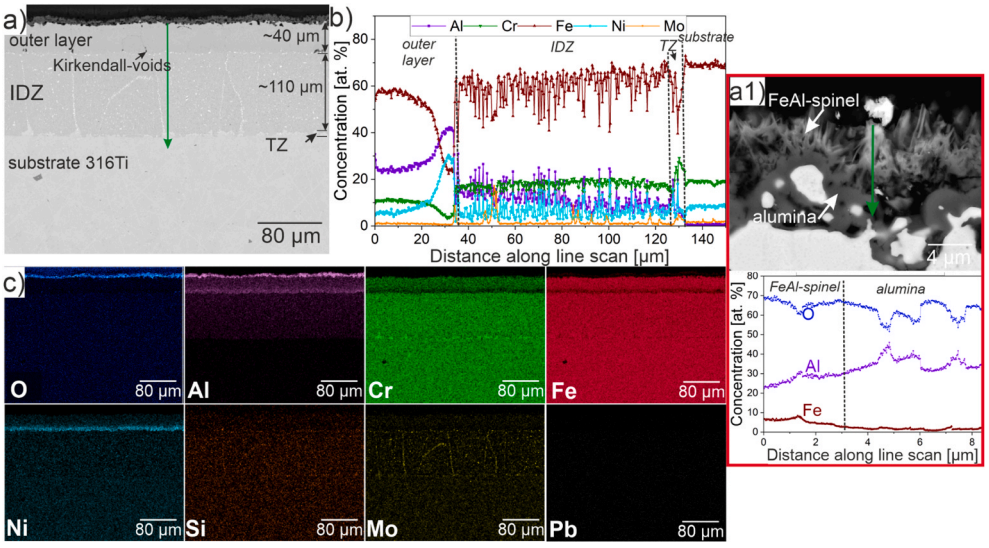

Fig. 13. Aluminized 316Ti pre-oxidized after 5000 h exposure in liquid Pb at 600 °C. a) Cross-sectional BSE image, b) EDS elemental line scan result (see green line in Fig a), c) EDS elemental distribution mapping result of a. Detail a1) enlarged section of oxide layer and the EDS line scan results across the oxide layer.

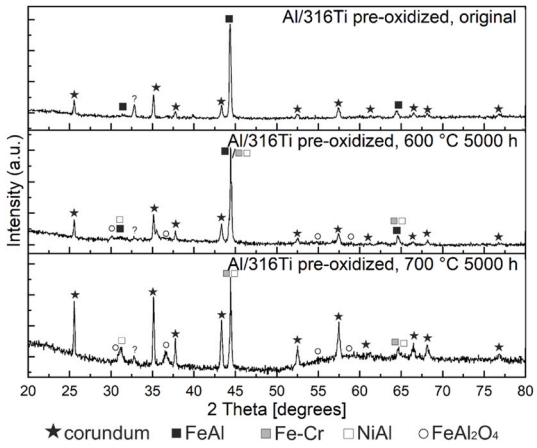

Fig. 14. XRD results of aluminized 316Ti pre-oxidized before and after 5000 h exposures in liquid Pb at 600 °C and 700 °C.

3.4. Aluminized 316Ti pre-oxidized

Fig. 13 shows the cross-sectional analysis of the aluminized 316Ti pre-oxidized after 5000 h exposure in liquid Pb at 600 °C (corresponding low-magnification image in Fig. S4b). No liquid Pb is detected in either the coating or the substrate. An oxide double layer is clearly visible, as depicted in Fig. 13a1: an outer needle-like Fe-Al spinel and an inner α-Al_2O_3 layer. Based on the XRD results presented in Fig. 14, the Fe-Al-rich oxide layer is identified as hercynite $FeAl_2O_4$. The presence of $FeAl_2O_4$ spinel on top of the alumina indicates that the alumina layer formed during the pre-oxidation process is not dense enough to completely prevent the outward diffusion of Fe. This is in contrast to alumina layers typically formed on the surface of Al-containing alloys during liquid Pb exposure at reduced temperature and oxygen activity (see, e.g., AFA steels, Kanthal, or aluminized 316Ti exposed at 600 °C in this study), which grow very slowly and form dense layers that completely prevent the outward diffusion of Fe. Despite its considerable total thickness of 8–10 μm, the Al-rich oxide layer observed here still adheres well to the aluminide layer. According to the EDS line scan in Fig. 13b, the Al concentration in the outer layer decreased slightly from 26 at% to 24 at%. Despite the reduced Al content, the outer layer remains homogeneous in microstructure throughout the entire sample, similar to the as-prepared sample at the location shown in Fig. 4b; no decomposition into an Al-reduced ferritic matrix and dispersed NiAl precipitates is observed as shown in Fig. 4d. Additionally, Mo-Si-rich carbides (χ-phase) formed within the ferritic matrix of the IDZ and a rather thin transition zone to the bulk material developed. A similar microstructural evolution of IDZ and transition zone was observed in the aluminized 316Ti specimen without pre-oxidation exposed at 600 °C for 2000 h, see Fig. 11.

As shown in Fig. 15a1, at an elevated exposure temperature of 700 °C, the oxide double layer comprising the $FeAl_2O_4$ spinel and the underlying α-Al_2O_3 layer grown on the coating is considerably thicker (10–13 μm in total) than the oxide layer at 600 °C. The oxide double layer exhibits local delamination and cracks. Nevertheless, no signs of liquid Pb penetration are observed (see Fig. 15a and Fig. S4c). Oxides are also found within the cracks and voids, and simultaneously, NiAl phase is observed to develop both within and around the cracks. The Kirkendall voids between the outer layer and the IDZ are larger than those observed during exposure at 600 °C. The microstructure of the outer layer is uniform across the sample. It consists of an Fe-Cr-Ni-Al matrix with ferritic structure (based on the XRD results in Fig. 14 and the EDS line scan results in Fig. 15b) and finely dispersed NiAl precipitates. The EDS line scan in Fig. 15b shows a depletion of the Al concentration to ~10 at% within the matrix, while the Fe concentration increases significantly to 70 at% and the Cr concentration exceeds 15 at%. This composition suggests a ferritic microstructure. Between the outer layer and the IDZ, a region with Ni- and Al-enrichment and Cr-depletion to 0.9 at% is present (see line scan in Fig. 15b and elemental mapping in Fig. 15c), which may correspond to B2-NiAl. Within the IDZ, Mo-Si-rich carbides (χ-phase) are formed at the inner ferritic grain boundaries. A 55 μm thick transition zone is observed below the IDZ, attributed to inward diffusion of Al into the substrate. Additionally, elongated NiAl precipitates are found in the transition region, along with the presence of a Cr-Mo-rich phase at the grain boundaries.

4. Discussion

The compatibility of austenitic stainless steel 316Ti with liquid Pb containing 2×10^{-7} wt% dissolved oxygen was investigated at two different temperatures, 600 °C and 700 °C. Thereby, the corrosion behavior of 316Ti without pre-treatment was compared with the behavior after three different pre-treatments: pre-oxidation, aluminizing by pack cementation, and aluminizing combined with pre-oxidation. Table 3 summarizes the corrosion test results qualitatively.

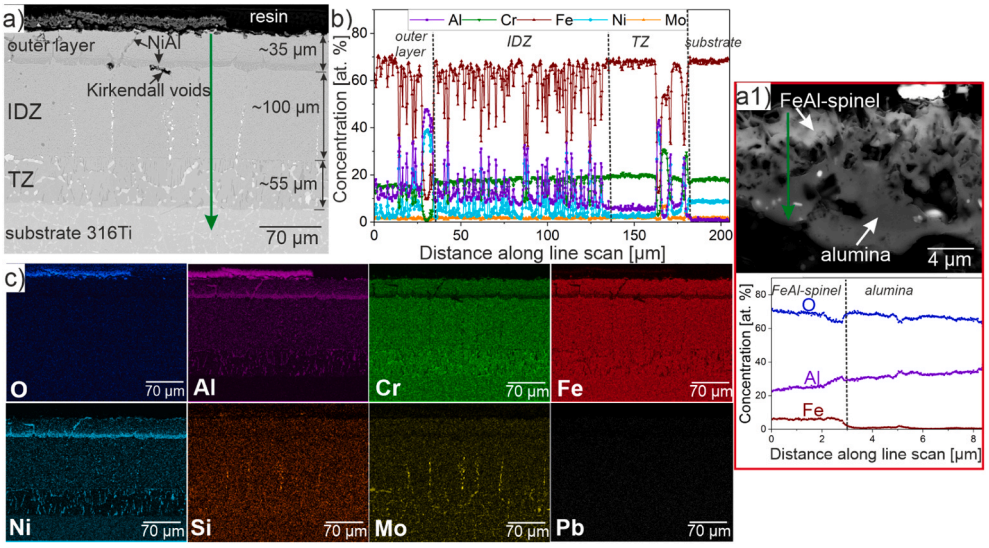

Fig. 15. Aluminized 316Ti pre-oxidized after 5000 h exposure in liquid Pb at 700 °C. a) Cross-sectional BSE image, b) EDS elemental line scan result (see green line in Fig a), c) EDS elemental distribution mapping result of a. Detail a1) enlarged section of oxide layer and the EDS line scan results across the oxide layer.

Table 3
Final assessment of 316Ti with different pre-treatments after exposures in liquid Pb. "–" indicates very poor corrosion resistance, "-" indicates poor corrosion resistance, and "++" indicates excellent corrosion resistance.

Material	600 °C			700 °C		
	1000 h	2000 h	5000 h	1000 h	2000 h	5000 h
Untreated 316Ti	–	–	–	-	-	-
316Ti pre-oxidized			++			-
Aluminized 316Ti	++	++		–	–	
Aluminized 316Ti pre-oxidized			++			++

Without any surface pre-treatment, 316Ti suffers from corrosion attack at both temperatures. At 600 °C, selective dissolution and Pb penetration reach a depth of 80 μm after 5000 h ("–" in Table 3). A slightly better corrosion resistance ("-") is obtained at the higher temperature of 700 °C. Thanks to the growth of a Cr-rich oxide at the sample surface in the initial stage of exposure, see also Ref. [11], the dissolution depth after 5000 h is reduced to 30 μm and no Pb penetration is observed. Evidently, the higher exposure temperature facilitates the outward transport of chromium and promotes the formation of a more protective Cr-rich scale compared to 600°C (compare Fig. 6 and Fig. 8). However, since further oxidation is not observed after the loss of the initial oxide (most probably due to the reduced Cr content in the subsurface region), a more severe corrosion attack with Pb penetration is expected also at 700 °C for prolonged exposure times.

Pre-oxidation in air (4 h at 1000 °C) considerably improves the corrosion resistance of 316Ti in liquid Pb, at least at 600 °C. The Cr-rich oxide grown during pre-oxidation, locally up to 50 μm deep, successfully protects the steel from dissolution corrosion (see Fig. 9). Although Pb is found in the pre-formed oxide, it does not reach the bulk material yet after 5000 h. The oxide formed during pre-oxidation does neither deteriorate visibly nor grow further during Pb exposure at 600 °C ("++" in Table 3). However, the Pb that penetrated into the pre-formed oxide bears the risk of dissolution corrosion for prolonged exposure. At 700 °C in liquid Pb, the pre-formed oxide further grows inward by selective oxidation of Cr and reaches a depth of 130 μm after 5000 h (Fig. 10). Although it still protects the steel from Pb penetration, local losses of the pre-formed Cr-rich oxide scale lead to selective dissolution of Ni and ferritization ("-"). To improve the corrosion resistance of pre-oxidized 316Ti in liquid Pb, an amended pre-oxidation treatment at a lower temperature (e.g., 800 °C [45]) or a gas atmosphere with reduced oxygen activity is recommended. This could help to form more dense and stable oxides (higher Cr content, no Ni) and to achieve a more homogeneous oxide scale thickness.

Although Cr-based oxides are preferred among the oxides of steel alloying elements for the high temperature oxidation/corrosion protection in liquid Pb and Pb alloys, they grow rather quickly at elevated temperature and can become permeable and/or porous, which deteriorates their protective properties. Therefore, Al-based oxides are favored. Their formation can be promoted by aluminizing the surface of 316Ti. In this study, aluminized 316Ti indeed shows the growth of an Al-rich oxide scale when exposed to liquid Pb with 2×10^{-7} wt% oxygen at 600 °C (see Fig. 11). The oxide phase could not be resolved with the utilized characterization techniques (TEM would be required) but is believed to be a transient alumina phase such as γ- or θ-Al_2O_3 [46]. The slowly growing oxide scale remains well below 1 μm after 2000 h and protects the material from corrosion attack, which indicates a dense, impermeable layer ("++" in Table 3). The excellent corrosion resistance of aluminized 316Ti at 600 °C is not at all reproduced at 700 °C. At the higher temperature, a strong corrosion attack with dissolution of steel alloying elements and Pb penetration to a depth of 180 μm after 2000 h is observed, see Fig. 12 ("–"). Responsible is the increased solubility of Al and steel alloying elements in Pb and enhanced dissolution kinetics at the higher temperature, which evidently predominate the also enhanced oxidation kinetics. Formation of an alumina layer even at 700 °C could probably be achieved by a higher amount of oxygen dissolved in the liquid Pb. Alternatively, an initial protection of the aluminide coating against dissolution at 700 °C can be provided by pre-oxidation of the aluminized 316Ti.

Aluminized 316Ti shows a 3–9 μm thick alumina scale with some internal cracks after 4 h of pre-oxidation in air at 1000 °C (see Fig. 4). Since thick alumina scales bear the risk of spallation, pre-oxidation with shorter duration is recommended. The high temperature is required to induce growth of stable α-alumina. Exposure of aluminized and pre-oxidized 316Ti to Pb at 600 °C leads to the formation of an additional needle-shaped Fe-Al spinel on top of the pre-formed alumina (Fig. 13). The total oxide scale thickness slightly increases to 8–10 μm after 5000 h. Despite the rather large thickness, the Al-rich oxide scale remains protective against corrosion attack. Neither dissolution nor Pb penetration are observed ("++" in Table 3). Although pre-oxidation of aluminized 316Ti has no benefit for the corrosion resistance at 600 °C, it does also not deteriorate the protection against corrosion. In case of oxide scale spallation after a longer exposure duration, re-healing of an Al-rich oxide scale is likely (as observed in the exposure without pre-oxidation).

At 700 °C, the condition at which the aluminized 316Ti without pre-oxidation experienced strong dissolution and Pb penetration (Fig. 12), pre-oxidation of the aluminized 316Ti greatly improves the corrosion resistance (see Fig. 15). The Fe-Al spinel that grows on the pre-formed alumina scale during Pb exposure at 700 °C is thicker than the spinel grown at 600 °C. A total oxide layer thickness of 10–13 μm is obtained after 5000 h. Although the oxide scale develops cracks due to its higher thickness at 700 °C, it still protects the material from dissolution and Pb penetration after 5000 h ("++"). This suggests that a thin protective oxide layer remains on the surface even in locations with delamination. Another possibility is that cracks and spallation occurred very late in the exposure test or when cooling down from the exposure temperature. Because of the high solubilities in Pb and enhanced dissolution kinetics at 700 °C as mentioned above, long-term corrosion tests are required to confirm the excellent corrosion resistance even in case of oxide scale spallation during exposure.

Regarding the expected long-term corrosion resistance and the mechanical integrity and strength of the aluminide coating, the evolution of the pack cementation coating itself is of great interest. At elevated temperature, diffusion of Al and steel alloying elements takes place, driven, on the one hand, by the differences in composition between coating and steel and, on the other hand, by surface processes and the contact with the adjacent environment. This applies to both the pre-oxidation step (4 h at 1000 °C) and the exposures to liquid Pb at 600 and 700 °C, respectively.

During pre-oxidation, the Al content of the outer layer significantly decreases from ~52 at% to ~26 at% and Kirkendall voids appear, while its thickness remains rather constant at ~40 μm. A decrease in Al content also occurs during Pb exposure at 600 °C, though at a much slower pace (2–4 at% reduction in 2000–5000 h) thanks to the lower oxidation rate at the lower temperature and the incorporation of Fe in the mixed Fe-Al spinel. This applies to both pre-oxidized and as-prepared aluminide coatings. Once the Al content drops below a certain value, the originally homogenous B2-type microstructure of the outer layer

decomposes into a ferritic matrix with further reduced Al content and NiAl precipitates. This is observed, for instance, for the pre-oxidized sample after 5000 h in liquid Pb at 700 °C. Here, only ~10 at% Al remains in the matrix of the outer layer, and its thickness is reduced to 35 μm. For prolonged exposure at elevated temperature, it is expected that the Al content of the outer layer further declines due to continued oxide formation and diffusion towards the bulk. Once the Al content of the matrix drops below a certain level, the NiAl precipitates are expected to act as reservoir and provide Al for the formation and potential re-healing of the oxide scale.

The interdiffusion zone strongly increases in thickness from ~55 μm to ~110 μm during pre-oxidation at 1000 °C, caused by Al diffusion towards the bulk. This effect could be reduced by a shorter pre-oxidation step. The microstructure of the IDZ remains rather unchanged, also at the transition to the bulk. In contrast, no change in IDZ thickness is observed during Pb exposure at 600 or 700 °C, but microstructural changes and formation of ferritic phases (Mo-Si-rich carbides, coarse Cr-Mo-rich precipitates, elongated NiAl) occur due to the much longer timescale of 1000–5000 h. The embrittlement of the alloy surface due to the presence of Al-rich intermetallic phases can reduce the creep strength [47]. To counter-act this, a tradeoff between the negative influence of the coating on the mechanical behavior of the component and the positive influence of it on the corrosion resistance in liquid Pb needs to be found in future studies by controlling the coating phases and its thickness by optimizing the pack cementation process.

5. Conclusion

Austenitic stainless steel 316Ti shows selective dissolution and Pb penetration to a depth of 80 μm after 5000 hours exposure at 600 °C to liquid Pb containing 2×10^{-7} wt% dissolved oxygen. A slightly improved corrosion resistance is obtained at 700 °C thanks to formation of a Cr-rich oxide scale in the initial stage. For prolonged Pb exposure, however, the oxide scale disappears and the steel 316Ti suffers from dissolution corrosion also at 700 °C. Therefore, the effectiveness of three different pre-treatments in improving the corrosion resistance of 316Ti in liquid Pb at 600–700 °C was investigated in corresponding exposure tests with duration up to 5000 h.

- Pre-oxidation of 316Ti in air at 1000 °C for 4 h caused the growth of an oxide layer containing Cr_2O_3 and mixed Fe, Cr, and Ni oxides. This oxide scale proved protective when the pre-oxidized 316Ti was exposed to liquid Pb at 600 °C. At 700 °C, however, the oxide further grew inwards and lost its protective properties against selective dissolution of steel alloying elements.
- Aluminizing of 316Ti by pack cementation resulted in the formation of an FeAl intermetallic phase at the sample surface. Like pre-oxidation, also aluminizing successfully improved the corrosion resistance of 316Ti at 600 °C only. A thin Al-rich oxide scale grew on the surface of the aluminized 316Ti and protected the steel against dissolution. At 700 °C, strong dissolution and Pb penetration occurred to a depth of 180 μm after 2000 h exposure.
- Pre-oxidation of previously aluminized 316Ti resulted in formation of an α-Al_2O_3 scale on the sample surface. The Al-oxide scale successfully protected the steel from corrosion attack in liquid Pb at both 600 °C and 700 °C. The very slow growth of an additional Fe-Al spinel on the sample surface promises excellent corrosion protection even for prolonged exposure.

From the presented results, application of a combined pre-treatment comprising aluminizing by pack cementation and subsequent pre-oxidation provides the best corrosion protection of the austenitic steel 316Ti when exposed at 600–700 °C to liquid Pb containing 2×10^{-7} wt % dissolved oxygen. This conclusion holds even though the pack cementation and pre-oxidation processes themselves were not optimized yet. Future work needs to include this parameter optimization for both processes and to investigate their effectiveness on other substrates.

CRediT authorship contribution statement

Purwitasari Anisa: Writing – original draft, Visualization, Investigation. **Müller Georg:** Resources, Project administration. **Heinzel Annette:** Writing – review & editing, Investigation. **Fetzer Renate:** Writing – review & editing, Writing – original draft. **Weisenburger Alfons:** Writing – review & editing, Supervision, Funding acquisition. **Oskay Ceyhun:** Writing – review & editing, Investigation.

Declaration of Competing Interest

The authors declare that they have no known competing financial interests or personal relationships that could have appeared to influence the work reported in this paper.

Acknowledgments

The authors express their gratitude to Melanie Thalheimer, Anke Silvia Ulrich, and Mathias Galetz for providing the pack aluminizing of 316Ti. This research was funded by the German Federal Ministry for Economic Affairs and Climate Actions (BMWK) under the grant number 03EE5050C.

Appendix A. Supporting information

Supplementary data associated with this article can be found in the online version at doi:10.1016/j.corsci.2025.112896.

Data Availability

Data will be made available on request.

References

[1] K. Niedermeier, A perspective on high-temperature heat storage using liquid metal as heat transfer fluid, Energy Storage 5 (2023) e530, https://doi.org/10.1002/est2.530.
[2] A. Heinzel, W. Hering, J. Konys, L. Marocco, K. Litfin, G. Müller, J. Pacio, C. Schroer, R. Stieglitz, L. Stoppel, A. Weisenburger, T. Wetzel, Liquid metals as efficient high-temperature heat-transport fluids, Energy Technol. 5 (2017) 1026–1036, https://doi.org/10.1002/ente.201600721.
[3] M.-J. Li, Y.-J. Jie, H.-H. Zhu, G.-J. Qi, M.-J. Li, The thermodynamic and cost-benefit-analysis of miniaturized lead-cooled fast reactor with supercritical CO2 power cycle in the commercial market, Prog. Nucl. Energy 103 (2018) 135–150, https://doi.org/10.1016/j.pnucene.2017.11.015.
[4] L. Miró, J. Gasia, L.F. Cabeza, Thermal energy storage (TES) for industrial waste heat (IWH) recovery: a review, Appl. Energy 179 (2016) 284–301, https://doi.org/10.1016/j.apenergy.2016.06.147.
[5] U. Pelay, L. Luo, Y. Fan, D. Stitou, M. Rood, Thermal energy storage systems for concentrated solar power plants, Renew. Sustain. Energy Rev. 79 (2017) 82–100, https://doi.org/10.1016/j.rser.2017.03.139.
[6] P. Hosemann, D. Frazer, E. Stergar, K. Lambrinou, Twin boundary-accelerated ferritization of austenitic stainless steels in liquid lead–bismuth eutectic, Scr. Mater. 118 (2016) 37–40, https://doi.org/10.1016/j.scriptamat.2016.02.029.
[7] R. Wang, X. Qiu, S. Gao, W. Liu, W. Li, Y. Li, Z. Tang, Corrosion behavior of 316 stainless steel arc parts in liquid lead at 650 °C under high oxygen concentrations, RSC Adv. 12 (2022) 32700–32707, https://doi.org/10.1039/D2RA05165F.
[8] C. Cionea, M.D. Abad, Y. Aussat, D. Frazer, A.J. Gubser, P. Hosemann, Oxide scale formation on 316L and FeCrAl steels exposed to oxygen controlled static LBE at temperatures up to 800°C, Sol. Energy Mater. Sol. Cells 144 (2016) 235–246, https://doi.org/10.1016/j.solmat.2015.09.007.
[9] J. Zhang, A review of steel corrosion by liquid lead and lead–bismuth, Corros. Sci. 51 (2009) 1207–1227, https://doi.org/10.1016/j.corsci.2009.03.013.
[10] A. Weisenburger, C. Schroer, A. Jianu, A. Heinzel, J. Konys, H. Steiner, G. Müller, C. Fazio, A. Gessi, S. Babayan, A. Kobzova, L. Martinelli, K. Ginestar, F. Balbaud-Célerier, F.J. Martín-Muñoz, L. Soler Crespo, Long term corrosion on T91 and AISI1 316L steel in flowing lead alloy and corrosion protection barrier development: experiments and models, J. Nucl. Mater. 415 (2011) 260–269, https://doi.org/10.1016/j.jnucmat.2011.04.028.
[11] A. Purwitasari, C. Oskay, A. Heinzel, R. Fetzer, A. Weisenburger, G. Müller, Corrosion of austenitic stainless steels in liquid Pb with 2E-7 wt% oxygen at 600 and 700 °C, Corros. Sci. 244 (2025) 112651, https://doi.org/10.1016/j.corsci.2024.112651.

[12] E.L. Maia, S. Gavrilov, V. Tsisar, K. Baert, I. De Graeve, Early stages of liquid-metal corrosion on pre-oxidized surfaces of austenitic stainless steel 316L exposed to static Pb-Bi eutectic at 400 °C, Corros. Sci. 227 (2024) 111680, https://doi.org/10.1016/j.corsci.2023.111680.
[13] B.A. Pint, J. Jun, Pre-oxidation to improve liquid metal compatibility, Oxid. Met. 96 (2021) 231–240, https://doi.org/10.1007/s11085-021-10057-4.
[14] H. Shi, A. Jianu, A. Weisenburger, C. Tang, A. Heinzel, R. Fetzer, F. Lang, R. Stieglitz, G. Müller, Corrosion resistance and microstructural stability of austenitic Fe–Cr–Al–Ni model alloys exposed to oxygen-containing molten lead, J. Nucl. Mater. 524 (2019) 177–190, https://doi.org/10.1016/j.jnucmat.2019.06.043.
[15] P. Dömstedt, M. Lundberg, P. Szakálos, Corrosion studies of a low alloyed Fe–10Cr–4Al steel exposed in liquid Pb at very high temperatures, J. Nucl. Mater. 531 (2020) 152022, https://doi.org/10.1016/j.jnucmat.2020.152022.
[16] H. Shi, R. Fetzer, C. Tang, D.V. Szabó, S. Schlabach, A. Heinzel, A. Weisenburger, A. Jianu, G. Müller, The influence of Y and Nb addition on the corrosion resistance of Fe-Cr-Al-Ni model alloys exposed to oxygen-containing molten Pb, Corros. Sci. 179 (2021) 109152, https://doi.org/10.1016/j.corsci.2020.109152.
[17] H. Shi, R. Fetzer, A. Jianu, A. Weisenburger, A. Heinzel, F. Lang, G. Müller, Influence of alloying elements (Cu, Ti, Nb) on the microstructure and corrosion behaviour of AlCrFeNi-based high entropy alloys exposed to oxygen-containing molten Pb, Corros. Sci. 190 (2021) 109659, https://doi.org/10.1016/j.corsci.2021.109659.
[18] K. Kishore, S. Chhangani, M.J.N.V. Prasad, K. Bhanumurthy, Microstructure evolution and hardness of hot dip aluminized coating on pure iron and EUROFER 97 steel: Effect of substrate chemistry and heat treatment, Surf. Coat. Technol. 409 (2021) 126783, https://doi.org/10.1016/j.surfcoat.2020.126783.
[19] E. Serra, H. Glasbrenner, A. Perujo, Hot-dip aluminium deposit as a permeation barrier for MANET steel, Fusion Eng. Des. 41 (1998) 149–155, https://doi.org/10.1016/S0920-3796(98)00224-5.
[20] G. Müller, A. Heinzel, J. Konys, G. Schumacher, A. Weisenburger, F. Zimmermann, V. Engelko, A. Rusanov, V. Markov, Results of steel corrosion tests in flowing liquid Pb/Bi at 420–600 °C after 2000h, J. Nucl. Mater. 301 (2002) 40–46, https://doi.org/10.1016/S0022-3115(01)00725-5.
[21] A. Heinzel, Korrosionsverhalten von Stählen in sauerstoffbeladenem, flüssigem Pb55,5%Bi unter Berücksichtigung von Oberflächenmodifikationen, Diss., FZKA 6823 (2003), https://doi.org/10.5445/IR/502003.
[22] G. Müller, A. Heinzel, J. Konys, G. Schumacher, A. Weisenburger, F. Zimmermann, V. Engelko, A. Rusanov, V. Markov, Behavior of steels in flowing liquid PbBi eutectic alloy at 420–600 °C after 4000–7200h, J. Nucl. Mater. 335 (2004) 163–168, https://doi.org/10.1016/j.jnucmat.2004.07.010.
[23] Z.D. Xiang, S.R. Rose, P.K. Datta, Long-term oxidation kinetics of aluminide coatings on alloy steels by low temperature pack cementation process, J. Mater. Sci. 41 (2006) 7353–7360, https://doi.org/10.1007/s10853-006-0806-0.
[24] B.L. Bates, Y.Q. Wang, Y. Zhang, B.A. Pint, Formation and oxidation performance of low-temperature pack aluminide coatings on ferritic–martensitic steels, Surf. Coat. Technol. 204 (2009) 766–770, https://doi.org/10.1016/j.surfcoat.2009.09.063.
[25] C. Boulesteix, V. Kolarik, F. Pedraza, Steam oxidation of aluminide coatings under high pressure and for long exposures, Corros. Sci. 144 (2018) 328–338, https://doi.org/10.1016/j.corsci.2018.08.053.
[26] A. Agüero, R. Muelas, A. Pastor, S. Osgerby, Long exposure steam oxidation testing and mechanical properties of slurry aluminide coatings for steam turbine components, Surf. Coat. Technol. 200 (2005) 1219–1224, https://doi.org/10.1016/j.surfcoat.2005.07.080.
[27] P. Audigié, V. Encinas-Sánchez, M. Juez-Lorenzo, S. Rodríguez, M. Gutiérrez, F. J. Pérez, A. Agüero, High temperature molten salt corrosion behavior of aluminide and nickel-aluminide coatings for heat storage in concentrated solar power plants, Surf. Coat. Technol. 349 (2018) 1148–1157, https://doi.org/10.1016/j.surfcoat.2018.05.081.
[28] B. Grégoire, C. Oskay, T.M. Meißner, M.C. Galetz, Corrosion performance of slurry aluminide coatings in molten NaCl–KCl, Sol. Energy Mater. Sol. Cells 223 (2021) 110974, https://doi.org/10.1016/j.solmat.2021.110974.
[29] P. Audigié, V. Encinas-Sánchez, S. Rodríguez, F.J. Pérez, A. Agüero, High temperature corrosion beneath carbonate melts of aluminide coatings for CSP application, Sol. Energy Mater. Sol. Cells 210 (2020) 110514, https://doi.org/10.1016/j.solmat.2020.110514.
[30] Ph Deloffre, F. Balbaud-Célérier, A. Terlain, Corrosion behaviour of aluminized martensitic and austenitic steels in liquid Pb–Bi, J. Nucl. Mater. 335 (2004) 180–184, https://doi.org/10.1016/j.jnucmat.2004.07.014.
[31] S. Majumdar, A. Borgohain, V. Kain, Interaction between liquid lead-bismuth eutectic and aluminized Inconel 625 superalloy at 600 and 850 °C, J. Nucl. Mater. 518 (2019) 54–61, https://doi.org/10.1016/j.jnucmat.2019.02.046.
[32] Z.D. Xiang, P.K. Datta, Relationship between pack chemistry and aluminide coating formation for low-temperature aluminisation of alloy steels, Acta Mater. 54 (2006) 4453–4463, https://doi.org/10.1016/j.actamat.2006.05.032.
[33] Y.Q. Wang, Y. Zhang, D.A. Wilson, Formation of aluminide coatings on ferritic–martensitic steels by a low-temperature pack cementation process, Surf. Coat. Technol. 204 (2010) 2737–2744, https://doi.org/10.1016/j.surfcoat.2010.02.025.
[34] E. Pauletti, A.S.C.M. d'Oliveira, Study on the mechanisms of formation of aluminized diffusion coatings on a Ni-base superalloy using different pack aluminization procedures, J. Vac. Sci. Technol. A 36 (2018) 041504, https://doi.org/10.1116/1.5026272.
[35] F. Bozza, G. Bolelli, C. Giolli, A. Giorgetti, L. Lusvarghi, P. Sassatelli, A. Scrivani, A. Candeli, M. Thoma, Diffusion mechanisms and microstructure development in pack aluminizing of Ni-based alloys, Surf. Coat. Technol. 239 (2014) 147–159, https://doi.org/10.1016/j.surfcoat.2013.11.034.
[36] G.W. Goward, D.H. Boone, Mechanisms of formation of diffusion aluminide coatings on nickel-base superalloys, Oxid. Met. 3 (1971) 475–495, https://doi.org/10.1007/BF00604047.
[37] Y. Zhang, B.A. Pint, K.M. Cooley, J.A. Haynes, Formation of aluminide coatings on Fe-based alloys by chemical vapor deposition, Surf. Coat. Technol. 202 (2008) 3839–3849, https://doi.org/10.1016/j.surfcoat.2008.01.023.
[38] B.A. Pint, Y. Zhang, P.F. Tortorelli, J.A. Haynes, I.G. Wright, Evaluation of iron-aluminide CVD coatings for high temperature corrosion protection, Mater. High. Temp. 18 (2001) 185–192, https://doi.org/10.1179/mht.2001.021.
[39] Y. Zhang, B.A. Pint, K.M. Cooley, J.A. Haynes, Effect of nitrogen on the formation and oxidation behavior of iron aluminide coatings, Surf. Coat. Technol. 200 (2005) 1231–1235, https://doi.org/10.1016/j.surfcoat.2005.07.081.
[40] F. Pedraza, M. Proy, C. Boulesteix, P. Krukovskyi, M. Metel, Slurry aluminizing of IN-800HT austenitic stainless steel and pure nickel. Correlations between experimental results and modelling of diffusion, Mater. Corros. 67 (2016) 1059–1067, https://doi.org/10.1002/maco.201508758.
[41] C. Lopez, A. Kvryan, S. Kasnakjian, A. Coronado, S. Sujittosakul, O. Villalpando, V. A. Ravi, Effect of austenite stability on pack aluminizing of austenitic stainless steels, JOM 67 (2015) 61–67, https://doi.org/10.1007/s11837-014-1238-y.
[42] G. Müller, G. Schumacher, F. Zimmermann, Investigation on oxygen controlled liquid lead corrosion of surface treated steels, J. Nucl. Mater. 278 (2000) 85–95, https://doi.org/10.1016/S0022-3115(99)00211-1.
[43] Handbook on Lead-bismuth Eutectic Alloy and Lead Properties, Materials Compatibility, Thermal-hydraulics and Technologies, OECD Publishing, Paris, 2015.
[44] K.M. Doleker, A. Erdogan, T. Yener, Investigation of the surface degradation properties of aluminized super austenitic stainless steel, JOM 76 (2024) 522–539, https://doi.org/10.1007/s11837-023-06196-5.
[45] H. Buscail, S. El Messki, F. Riffard, S. Perrier, C. Issartel, Effect of pre-oxidation at 800 °C on the pitting corrosion resistance of the AISI 316L stainless steel, Oxid. Met. 75 (2011) 27–39, https://doi.org/10.1007/s11085-010-9218-2.
[46] A. Agüero, M. Hernández, A. Santaballa, Effects of a steam pre-treatment on the formation and transformation of alumina phases on Fe aluminide coatings, Oxid. Met. 79 (2013) 601–611, https://doi.org/10.1007/s11085-012-9351-1.
[47] B.L. Bates, Y. Zhang, S. Dryepondt, B.A. Pint, Creep behavior of pack cementation aluminide coatings on Grade 91 ferritic–martensitic alloy, Surf. Coat. Technol. 240 (2014) 32–39, https://doi.org/10.1016/j.surfcoat.2013.12.008.